Epigenetic adaptation drives monocyte differentiation into microglia-like cells upon engraftment into the retina

Jie Liu[a*], Fengyang Lei[a*], Bin Yan[a,b] , Naiwen Cui[c], Jyoti Sharma[a], Victor Correa[a], Lara Roach[d], Savvas Nicolaou[a], Kristen Pitts[a], James Chodosh[e], Daniel E. Maidana[f], Demetrios Vavvas[a], Milica A Margeta[a] , Huidan Zhang[c], David Weitz[c], Raul Mostoslavsky[d], and Eleftherios I. Paschalis[a]

a. Department of Ophthalmology, Massachusetts Eye and Ear, Harvard Medical School, Boston, MA 02114, USA
b. Department of Ophthalmology, The Second Xiangya Hospital of Central South University, 139 Middle Renmin Road, Changsha, Hunan, 410011, China
c. School of Engineering and Applied Sciences (SEAS), Harvard University, Cambridge, MA, USA.
d. Center for Regenerative Medicine, Massachusetts General Hospital, Harvard Medical School, Boston, MA 02114, USA
e. Department of Ophthalmology and Visual Sciences, University of New Mexico School of Medicine, Albuquerque, NM 87131, USA
f. Department of Ophthalmology and Visual Sciences, Illinois Eye and Ear Infirmary, University of Illinois at Chicago, Chicago, IL

*Equal contribution

Corresponding author: Eleftherios I. Paschalis
Email: eleftherios_paschalis@meei.harvard.edu

Author Contributions: J.L. and E.I.P. designed research; J.L., F.L., N.C. and B.Y. performed research; J.L., F.L., N.C., S.N. and J.S.,V.C., S.N., D.V., D.W., R.M. and M.A.M. analyzed data; and J.L., B.Y., J.C., D.E.M., D.V., D.W., R.M. and E.I.P. wrote the paper.

Competing Interest Statement: The authors declare no competing interest.

Classification: Biological Science/Immunology and Inflammation.
Keywords: microglia, marker, macrophages, monocytes, retina

Funding: Boston KPro Fund, NIH 5P30EY003790.

This file includes:
Main Text
Figures 1 to 6 and S1 to 4
Tables 1

Abstract

The identification of specific markers for microglia has been a long-standing challenge. Recently, markers such as P2ry12, TMEM119, and Fcrls have been proposed as microglia-specific and widely used to explore microglial functions within various central nervous system (CNS) contexts. The specificity of these markers was based on the assumption that circulating monocytes retain their distinct signatures even after infiltrating the CNS. However, recent findings reveal that infiltrating monocytes can adopt microglia-like characteristics while maintaining a pro-inflammatory profile upon permanent engraftment in the CNS.In this study, we utilize bone marrow chimeras, single-cell RNA sequencing, ATAC-seq, flow cytometry, and immunohistochemistry to demonstrate that engrafted monocytes acquire expression of established microglia markers—P2ry12, TMEM119, Fcrls—and the pan-myeloid marker Iba1, which has been commonly mischaracterized as microglia-specific. These changes are accompanied by alterations in chromatin accessibility and shifts in chromatin binding motifs that are indicative of microglial identity. Moreover, we show that engrafted monocytes dynamically regulate the expression of CX3CR1, CCR2, Ly6C, and transcription factors PU.1, CTCF, RUNX, AP-1, CEBP, and IRF2, all of which are crucial for shaping microglial identity. This study is the first to illustrate that engrafted monocytes in the retina undergo both epigenetic and transcriptional changes, enabling them to express microglia-like signatures. These findings highlight the need for future research to account for these changes when assessing the roles of monocytes and microglia in CNS pathology.

20 **Significance Statement**

21

22 Monocytes can express putative microglia markers P2ry12, TMEM119, and Fcrls upon
23 engraftment into the retina. Given their involvement in neuroinflammation, it is crucial to
24 consider this overlap when utilizing these markers for experimental analysis.

Introduction

Microglia and infiltrating peripheral monocytes play a central role in central nervous system (CNS) pathology and have become therapeutic targets in recent studies [1-5]. Given that these immune cell populations have overlapping biological functions, the use of markers for their differentiation often results in the inadvertent mislabeling, thereby compromising interpretation of relevant experimental data. More recently, P2ry12, TMEM119, and Fcrls were proposed as microglia "specific" markers and subsequently used in various studies[6, 7]. The specificity of these markers was originally assessed by comparing their expression in blood, spleen, or infiltrating monocytes against that of CNS-resident microglia. It was presumed that infiltrating monocytes would maintain their distinct characteristics following infiltration into the CNS and preserve these features for the long-term after engraftment into the tissue [6, 7].

However, recent findings indicate that infiltrating monocytes undergo persistent phenotypic changes upon engraftment into the CNS [2, 8]. These changes not only make them morphometrically similar to microglia but also allow them to permanently engraft into the tissue and live for the long-term, while retaining a pro-inflammatory that that can ultimately promote disease [2]. In previous studies, we identified "infiltrating monocytes" as ameboid, CCR2^{hi} CX3CR1^{lo} cells during the early infiltration phase (0-3 days), while engrafted monocytes were classified as ramified, CX3CR1^{hi} CCR2^{lo} cells typically migrating into distinct microglia strata [2].

In this study, we explore the ability of peripheral monocytes to express the putative microglia markers P2ry12, TMEM119, and Fcrls upon engraftment into the retina, and we investigate the mechanisms driving this phenotypic switch. We demonstrate that shortly after engraftment, monocytes begin expressing P2ry12, TMEM119, and Fcrls, while simultaneously undergoing dynamic changes in chromatin accessibility, binding motifs, and their transcriptome. This context-dependent adaptation allows engrafted monocytes not only to express microglia markers but also to modulate the expression of conventional monocyte/macrophage markers such as CX3CR1, CCR2, Ly6C, and key transcription factors including PU.1, CTCF, RUNX, AP-1, CEBP, and IRF2, which are crucial for reshaping their identity towards a microglia-like state.

This study highlights the significant plasticity of monocytes, showing that these cells can rapidly acquire microglia-like signatures upon engraftment into the retina. Distinguishing

56 between embryonic microglia and monocyte-derived “microglia” is essential for understanding
57 the distinct roles and functions of these two immune cell populations.
58

Results

Single-cell RNAseq reveals a transcriptional shift of engrafted monocytes towards a microglia signature.

Isolated CD45$^+$ CD11b$^+$ cells from the retina of wild-type mice were subjected to single-cell RNAseq prior to and 1, 4 and 7 days after ocular alkali injury. We previously showed that alkali injury to the cornea causes prompt infiltration of CCR2$^+$ monocytes and their subsequent engraftment into the retinal tissue[2, 9]. Using t-SNE we analyzed 954 cell/sample and identified 4 clusters with unique transcriptional profiles **(Fig. 1 A)**. Cluster 1 corresponded to yolk sack-derived native microglia, since prior to injury, peripheral monocytes do not infiltrate the retina[2-4, 9, 10]. One day after injury, monocytes and microglia formed two separate clusters; cluster 3 had high expression of Siglec1 gene, a monocyte marker [11-13] while cluster 4 had low expression, most indicative of microglia **(Fig. 1 B)**. At 4 days, microglia and monocytes formed a single cluster 2, suggestive of transcriptional overlap and at day 7, both cell populations were contained within cluster 1 (yolk-sac derived naïve microglia) **(Fig. 1 A)**, demonstrating a dynamic shift towards microglia signature. Gene expression analysis revealed the uniform expression of classical macrophage marker CX3CR1 in all clusters and predominant expression of CCR2 monocyte marker in cluster 2 (day 1) and 4 (day 4), **(Fig. 1 C, D)**. P2ry12 was highly expressed in cluster 1 (day 0 and 7) and 2 (day 4), TMEM119 and Fcrls in all clusters **(Fig. 1 C, D)**, and Aif1 (gene of IBA1) in cluster 2 (day 4). P2ry12 expression exhibited temporal regulation in monocytes, with lack of expression in clusters 3 and 4 – both representing early-stage infiltration (Day 1) **(Fig. 1 C, D)**. Next, a CX3CR1$^{+/EGFP}$ bone marrow chimera model was employed, as previously described[2, 4, 14], to differentiate the two immune cell populations (monocytes/microglia) using flow cytometry. Seven days after injury, engrafted CX3CR1$^+$ cells had adopted a similar CD45 expression as embryonic microglia, corroborating scRNAseq results of converging signature **(Fig. 1E)**. The results of scRNAseq were further confirmed using qPCR on bone marrow chimeras, which showed that monocytes acquire expression of P2ry12, TMEM119, Fcrls, and Iba1 genes within 45 days of engraftment **(Fig. S1)**. In contrast, embryonic microglia retained their expression in naïve and injured eyes **(Fig. S1)**.

Monocytes acquire de-novo expression of P2ry12, Fcrls, and TMEM119 in the protein level upon engraftment into the retina.

To determine whether the observed transcriptional changes in P2ry12, TMEM119, Fcrls, and IBA1 expression translate to the protein level in engrafted monocytes, we performed dual flow cytometry and immunohistochemistry analysis using a CX3CR1$^{+/GFP}$::CCR2$^{+/RFP}$ bone marrow chimera[2, 4, 14]. We first studied the CX3CR1$^{+/GFP}$::CCR2$^{+/RFP}$ double transgenic mouse to confirm that circulating monocytes (before engraftment) do not express P2ry12, TMEM119, or Iba1 in the protein level **(Fig. S2)**. We also confirmed that circulating monocytes express MHC-II **(Fig. S2)**. Using flow sorting of CD45^{+} CD11b^{+} CX3CR1^{+} blood cells from naïve mice, we confirmed the absence of Fcrls protein in circulating monocytes **(Fig. 2 C).**

One- and seven-days post-injury, GFP^{+} engrafted monocytes had no detectable expression of P2ry12 (white arrow), **(Fig. 2 A)**. By day 14, engrafted monocytes have transformed to ramified monocytes, acquired expression of P2ry12 and appearing morphometrically similar to microglia **(Fig. S3)**. At 45 days, engrafted monocytes had heterogeneous expression of P2ry12 with either positive or negative P2ry12 protein expression with approximately 55% of GFP^{+} engrafted monocyte being P2ry12 positive **(Fig. 2 A)**. The percentage of P2ry12 positive cell significantly increased compared to 1-day post-injury **(Fig. 2 A).** In contrast, embryonic microglia (GFP^{-}) retained robust expression of P2ry12 protein (yellow arrow) throughout the study period **(Fig. 2 A)**.

Likewise, 25% of GFP^{+} peripheral monocytes (white arrow) expressed TMEM119 at 1-day post-injury **(Fig. 2 B)**. By day 7, all GFP^{+} engrafted monocytes were TMEM119^{+}, and this expression was sustained on day 45 of engraftment **(Fig. 2 B).** The percentage of TMEM119 positive cell significantly increased compared to 1-day post-injury **(Fig. 2 B).** GFP^{-} embryonic microglia (yellow arrow) displayed robust expression of TMEM119 protein throughout the study period **(Fig 2 B)**.

Expression of Fcrls was assessed in CX3CR1$^{+/EGFP}$::CCR2$^{+/RFP}$ bone marrow chimeras by flow cytometry. First, CX3CR1^{+} cells were labeled with a conjugated antibody against CX3CR1 (BV605 or APC). BV605^{+}GFP^{-} or APC^{+} GFP^{-} cells were classified as embryonic microglia, and BV605^{+}GFP^{+} or APC+ GFP^{+} were classified as infiltrating peripheral monocytes **(Fig 2 C)**. Consistent with the above-mentioned findings, Fcrls was not expressed in blood monocytes (grey)[6], though 1 day after infiltration into the retina. BV605^{+}GFP^{+}

119 peripheral monocytes (purple) acquired higher expression of Fcrls as compared to embryonic
120 microglia at baseline **(Fig 2. C, D)**. In parallel, microglia reduced Fcrls expression below their
121 baseline level **(Fig. 2 C, D)**. Peripheral monocytes sustained high Fcrls expression at 7 days,
122 as compared to baseline microglia. By 45 days after injury, this expression was not
123 significantly different between embryonic microglia and engrafted monocytes **(Fig. 2 C, D)**.
124 Fcrls expression waned in infiltrating monocytes and increased in microglia after injury,
125 reaching similar levels at 45 days between these two immune populations, which was
126 equivalent to that of naive microglia at baseline **(Fig. 2 D)**.
127 IBA1 was expressed in GFP^+ monocytes (white arrow) already 1 day after engraftment
128 into the retina, with 85% of the cells being $IBA1^+$. By day 7, all GFP^+ engrafted monocytes
129 were expressing IBA1 and retained that expression until day 45 **(Fig. S4)**. GFP^- embryonic
130 microglia (yellow arrow) displayed robust expression of IBA1 throughout the study period **(Fig**
131 **S4)**.
132
133 **Monocytes undergo chromatin accessibility changes upon engraftment into the retina.**
134 Perturbances in tissue homeostasis often result in gene regulation and chromatin
135 accessibility changes with subsequent transcription/translation reshaping of key proteins in
136 monocytes [15-17]. Here, we employed the Assay for Transposase-Accessible Chromatin
137 with sequencing (ATAC-seq) to study the effect of monocyte engraftment in gene accessibility
138 for putative microglia markers P2ry12, Fcrls, TMEM119, and Iba1 in flow-sorted microglia and
139 peripheral monocytes using a bone marrow chimera model **(Fig. 2 A)**.

140 In ATAC seq, Peak width refers to the horizontal extent of a peak in the ATAC-seq signal
141 track. It represents the range over which chromatin accessibility is elevated. A wider peak
142 indicates a broader region of accessible chromatin. Peak amplitude refers to the height or
143 intensity of the peak in the ATAC-seq signal track. It represents the level of chromatin
144 accessibility at the peak's center. Higher amplitude suggests more frequent chromatin
145 accessibility in that region. In the current study, circulating monocytes and naïve microglia
146 were used as controls. Groups and color coding are listed in **(Fig. 3 A)**. Engrafted monocytes
147 showed similar open chromatin peaks to circulating monocytes (blue arrows) but also
148 displayed new open chromatin peaks not previously present in circulating monocytes (red
149 arrows) but present in native (embryonic) microglia. One of the peaks under the P2ry12 gene

150 in naïve microglia (red arrow) was absent in circulating monocytes but acquired upon
151 engraftment into the retina **(Fig. 3 B)**. The Fcrls gene had similar open chromatin peak across
152 all groups **(Fig. 3 C)**, though naïve microglia had wider and higher peak as compared to
153 circulating monocytes (blue peak compared to grey). After engraftment, the amplitude of this
154 peak increased in monocytes and became similar to microglia at day 45 (blue peak compared
155 to purple), **(Fig. 3 C)**. Similarly, TMEM119 chromatin was not accessible in circulating
156 monocytes, however, it became accessible after monocyte engraftment into the retina (red
157 arrow), **(Fig. 3 D)**. Lastly, AIF1 gene (IBA1) had similar open chromatin peaks among the
158 groups, corroborating the above transcriptional and protein findings showing gain of IBA1
159 expression by monocytes after engraftment into the retina **(Fig. 3 E)**.

160 Differential chromatin accessibility peaks were identified by comparing blood monocytes
161 to naive microglia or engrafted monocytes at 7 or 45 days. Heatmap analysis displayed
162 significant alterations in chromatin accessibility between the samples **(Fig. 3 F)** with more than
163 3000 differential chromatin accessibility peaks identified between peripheral and engrafted
164 monocytes at 7 days. These peak profiles remained stable at 45 days. Similarities in chromatin
165 accessibility between engrafted monocytes and microglia confirm our hypothesis that gradual
166 transition of chromatin state in engrafted monocytes facilitates their adaptation into the retina
167 **(Fig. 3 F)**.

168 Motif analysis of differential chromatin accessibility peaks was performed to identify the
169 most highly enriched transcription factor recognition motifs between circulating monocyte and
170 naive microglia or engrafted monocytes at 7 or 45 days. We identified motifs assigned to PU.1
171 (most dominant), CTCF, IRF, RUNX, MEF2, C/EBP, AP-1 in naive microglia, corroborating
172 previous findings [18] apart from motifs for MAF and MEF which were previously shown only
173 in microglia. In addition, we found other enriched motifs, including STAT1, FOXN1, KLFs,
174 ATF3, and Npas4, which have been reported to be associated with microglia functions of
175 polarization, cytokine production, suppression of inflammation and phagocytosis (22-26) **(Fig.
176 4)**. Engrafted monocytes had highly enriched motifs assigned to the above-mentioned
177 transcription factors, which we summarized in **Fig. 4**. In addition, engrafted monocytes
178 exhibited enriched motifs assigned to MITF and NFKB1, known to be responsible for disease-
179 associated transcriptional signatures [19] and promotion of inflammation, respectively **(Fig.
180 4)**. ATAC-seq analysis suggests that monocytes undergo dynamic open chromatin

accessibility changes upon engraftment into the retina, which affects their phenotype and allows them to acquire putative microglia signatures, although they remain somewhat functionally distinct in terms of promoting retinal neurodegeneration [2].

Monocytes undergo extensive changes in protein expression upon engraftment into the retina.

Further characterization of the protein expression changes in engrafted monocytes was performed using established markers Ly6C, CD45, and MHC-II in CX3CR1$^{+/GFP}$::CCR2$^{+/RFP}$ bone marrow chimeras **(Fig. 5 A).** Infiltrating monocytes (CD45^{+} CD11b^{+}) were CCR2^{high} CX3CR1^{low} at day 1 (Group 1), **(Fig. 5 B)**, and by day 7 were either CCR2^{high} CX3CR1^{low} (Group 2) or CCR2^{+} CX3CR1^{hi} (Group 3). At 45 days, engrafted monocytes were CCR2$^{low/-}$ CX3CR1^{high} (Group 5) with a small subpopulation being CCR2^{high}CX3CR1^{high} (Group 4), **(Fig. 5 B)**. CX3CR1^{-GFP} -negative CX3CR1^{-APC} -positive microglia were isolated 45 days after injury as controls (flow cytometry staining Group 6), **(Fig. 5 B)**.

CCR2^{high} monocytes displayed high expression of Ly6C at day 1, which gradually declined as cells transitioned to CCR2$^{low/-}$ CX3CR1^{high} during engraftment (Group 5), **(Fig. 5 C, D)**. In contrast, engrafted monocytes that retained CCR2^{high}CX3CR1^{high} expression also displayed sustained elevated expression of Ly6C throughout the study period (Group 4) **(Fig. 5 C, D)**. CD45 expression was similar to CCR2 expression; both markers were repressed in monocytes during engraftment **(Fig 5 E, F)**. The expression patterns of P2ry12, TMEM119, Fclrs, IBA1, CCR2, CX3CR1, Ly6C, and CD45, with monocyte and microglia morphometric characteristics[20] are summarized in (**Fig. 6)**.

Discussion

The exact role of microglia in central nervous system (CNS) pathology remains a subject of ongoing scientific debate. Numerous studies have reported both protective and deleterious roles for microglia across various CNS diseases, adding complexity to our understanding of their function [21-25]. This debate is compounded by technical limitations and the lack of specificity in microglia/monocyte markers, making it difficult to distinguish between these two immune cell populations [21, 22]. The challenge is further heightened by the ability of peripheral monocytes to infiltrate the CNS during disease, engraft permanently, and adopt a microglia-like morphology, complicating the identification of these cells[2]. Fate mapping studies have revealed that engrafted monocytes tend to exhibit a more pro-inflammatory phenotype compared to resident microglia[2, 26], emphasizing the critical need for accurate differentiation between these cell types in research studies. However, the absence of definitive markers has exacerbated the complexity of this issue.

Recently, markers such as P2ry12, FCRLS, TMEM119, and Iba1 were proposed as microglia-specific and have been rapidly adopted by the research community[6, 7, 27, 28]. Despite their widespread use, uncertainties persist regarding the specificity of these markers, particularly in the context of monocyte engraftment into CNS tissue. In this study, we utilized single-cell RNA sequencing, ATAC sequencing, and protein analysis to evaluate the expression of P2ry12, FCRLS, TMEM119, and Iba1 in engrafted monocytes within the retina, and to explore the chromatin accessibility changes that may contribute to the phenotypic switch observed in these cells.

TMEM119 has been highlighted as a promising microglia-specific marker, particularly in models of optic nerve injury, where it was shown to differentiate microglia from infiltrating $CCR2^{RFP/+}$ peripheral monocytes [7]. However, it has also been demonstrated that $CCR2^{-}$ $TMEM119^{+}$ peripheral monocytes can populate the injured optic nerve and contribute to the inflammatory environment [2, 4]. Our findings confirm that, in addition to microglia, CCR2+ $CX3CR1^{+}$ engrafted monocytes express TMEM119 as early as one day post-injury, with sustained expression at 45 days. These results align with previous reports of TMEM119 expression in other tissues [29, 30], raising important questions about the interpretation of data from past studies.

236 Additionally, P2ry12 and Fcrls have emerged as potential microglia-specific markers, but
237 their specificity was initially assessed by comparing CNS-derived $CD45^{lo}$ $CD11b^{+}$ microglia with
238 splenic CD11b+ Ly6C+ monocytes in naïve adult mice[6]. This comparison did not account for
239 engrafted monocytes. Additional studies using models of autoimmune encephalitis (EAE)
240 suggested that P2ry12 and Fcrls were not expressed in infiltrating monocytes during early EAE
241 onset[6]. However, our data show that both markers are indeed expressed by peripheral
242 monocytes after engraftment into the retina. Fcrls is expressed as early as one day post-injury,
243 with sustained expression, while P2ry12 is differentially expressed starting 14 days post-
244 engraftment, with some monocytes retaining P2ry12 expression throughout the study period.
245 These findings challenge the current understanding of these markers and suggest that previous
246 studies may need reevaluation, particularly in the context of neurodegenerative diseases such
247 as Alzheimer's, where P2ry12-negative microglia have been reported surrounding Aβ plaques
248 [31, 32]. Our data suggest that these cells could instead be engrafted monocytes, further
249 complicating the interpretation of microglia-specific roles in such contexts.
250 Although Iba1 is a well-known pan-myeloid marker, it has been frequently misused as a
251 microglia-specific in studies of tauopathy and multiple sclerosis [29, 32-38]. Using bone
252 marrow chimeras, we confirmed that Iba1 is expressed in both microglia and engrafted
253 monocytes, indicating that it should not be used to differentiate these immune cell populations.
254 Similarly, conventional markers like $CD45^{lo}$ and $CD11c^{lo}$, previously proposed to distinguish
255 microglia from peripheral monocytes/macrophages [39], proved inefficient in our study.
256 Specifically, the $CD45^{hi}$ $CD11b^{+}$ signature, often used for differentiation, was inadequate
257 outside the very acute phase of the experiment, as the majority of engrafted monocytes
258 repressed CD45 expression within 45 days, reaching levels comparable to $CD45^{lo}$ $CD11b^{+}$
259 microglia, as shown in this study and by others [39, 40].
260 Mechanistically, the expression of P2ry12, FCRLS, TMEM119, and Iba1 in engrafted
261 monocytes is associated with chromatin changes that enhance the accessibility of these
262 genes. Our ATAC-seq analysis revealed that engrafted monocytes undergo significant
263 chromatin accessibility changes, allowing them to acquire epigenetic signatures similar to
264 those of microglia. Additionally, other established microglia genes, such as SPP1, C1qa, and
265 Ms4a7, become accessible after monocyte engraftment, a feature not observed in circulating

266 blood monocytes. Whether these changes in chromatin accessibility translate to
267 transcriptional and protein-level expression requires further investigation [22, 40].
268 Understanding the molecular mechanisms that enable engrafted monocytes to acquire
269 microglia signatures is crucial for advancing our knowledge of neuroglia remodeling. Previous
270 studies have shown that transcription factors PU.1 (SPI-1) and Irf8 are essential for
271 microgliogenesis, while Batf3 and Klf4 are not [41]. Our motif analysis between circulating and
272 engrafted monocytes identified enriched transcription factor recognition motifs associated with
273 PU.1, CTCF, IRF, RUNX, MEF2, C/EBP, AP-1 (JUN/FOSB/BATF3), and MAF, present in both
274 human and mouse microglia [18]. This indicates a dynamic shift in the transcriptional network
275 that supports the differentiation of engrafted monocytes into microglia. Interestingly, while
276 SALL1 and SMAD4 have been implicated in microglia development and the expression of
277 P2ry12 and TMEM119 [42], these motifs were not enriched in our dataset, suggesting that
278 their role in monocyte identity transformation after engraftment may be less significant than
279 previously thought. Future studies should further explore the biological roles of the
280 transcription factors identified in our motif analysis.
281 There are limitations to this study that should be acknowledged. The use of a bone marrow
282 chimera model was necessary to differentiate microglia from engrafted monocytes. While this
283 model achieves stable chimerism and preserves blood-retinal barrier integrity, it requires
284 myeloablation and conditioning, which may affect hematopoiesis. We previously showed that
285 busulfan meylodepletion achieves stable chimerism and preserves blood-retinal barrier
286 integrity[2]. A parabiosis model, although potentially more reliable, is limited by low-level
287 chimerism [43]. Additionally, while we provide data on chromatin accessibility using ATAC-
288 seq, further experiments employing techniques like CUT&RUN [44] or ChIP-seq [18] would
289 be valuable in elucidating the epigenetic mechanisms governing gene expression in engrafted
290 monocytes and microglia. Another limitation is the need to explore whether our findings are
291 applicable to other CNS compartments, such as the brain, as marker expression may vary
292 across different tissues and pathological contexts.
293 Despite demonstrating that infiltrating monocytes can acquire microglia signatures at the
294 epigenetic, transcriptional, and protein levels, these cells remain distinct by expressing higher
295 levels of inflammatory cytokines, such as TNF-α and IL-1β, compared to resident microglia
296 [2]. Moreover, they exhibit enriched motifs associated with disease-associated and pro-

297 inflammatory transcription factors MITF and NFKB1, respectively [19, 45]. Therefore, further
298 analysis is required to fully delineate the functional differences between infiltrating monocytes
299 and microglia in the diseased CNS.

300 In conclusion, the implementation of newly developed microglia markers requires careful
301 validation to avoid misinterpretation of experimental data. While transgenic and lineage-
302 tracing models offer short-term solutions [2, 8, 46, 47], the development of reliable protein
303 markers are essential for long-term progress in the field. Until such markers are established,
304 the scientific community must remain vigilant about potential pitfalls when interpreting both
305 existing and new data.
306
307

Materials and Methods

Bone-Marrow Chimera Mouse Model. All animal-based procedures were performed in accordance with the Association for Research in Vision and Ophthalmology Statement for the Use of Animals in Ophthalmic and Vision Research. This study was approved by the Animal Care Committee of the Massachusetts Eye and Ear Infirmary. Mice were bred in-house at the Massachusetts Eye and Ear Animal Facility and were used at the age of 6–12 wk.

A CX3CR1$^{+/GFP}$::CCR2$^{+/RFP}$ bone marrow transfer model was used to distinguish periphery infiltrated monocytes from CNS resident microglia [2]. Briefly, C57BL/6J mice (Recipient mice) were myelodepleted with three i.p. injections of busulfan (35 mg/kg; Sigma-Aldrich), an alkylating agent that depletes bone-marrow cells, 7, 5, and 3 d before BMT. CX3CR1$^{+/EGFP}$::CCR2$^{+/RFP}$ (donor mice) bone-marrow cells (5 x 10^6 total bone-marrow cells) were transferred to the myelodepleted C57BL/6J mice through tail vein injection 1 month before corneal alkali burn. Bactrim (trimethoprim/sulfamethoxazole resuspended in 400 mL drinking water) was given ad libitum for 15 days after busulfan treatment.

Recipient mice C57BL/6J (stock no. 000664), and breeder mice including B6.129(Cg)-Ccr2tm2.1Ifc/J mice (stock no. 017586) and B6.129PCx3cr1tm1Litt/J mice (stock no. 005582) were obtained from Jackson Laboratory. Donor mice CX3CR1$^{+/EGFP}$::CCR2$^{+/RFP}$ mice were generated by breeding male B6.129(Cg)-Ccr2tm2.1Ifc/J mice with female B6.129PCx3cr1tm1Litt/J.

Mouse Model of Alkali Burn. One month after the CX3CR1$^{+/GFP}$::CCR2$^{+/RFP}$ bone marrow transfer model was established, corneal alkali chemical burns were performed according to our previous study [2]. In brief, mice were anesthetized using ketamine (60 mg/kg) and xylazine (6 mg/kg), and deep anesthesia was confirmed by toe pinch. A proparacaine hydrochloride USP 0.5% ophthalmic solution (Bausch and Lomb) was applied to the cornea and after 1 min was carefully dried with a Weck- Cel (Beaver Visitec International, Inc.). A 2-mm-diameter filter paper was soaked in 1 M sodium hydroxide (NaOH) solution for 10 s, dried of excess alkali, and applied onto the mouse cornea for 20 s. After the filter paper was removed, prompt irrigation with sterile saline was applied for 10 s. The mouse was then positioned laterally on a heating pad, and the eye was irrigated for another 15 min at low

339 pressure using sterile saline. Ethiqa XR (buprenorphine) extended-release injectable
340 suspension (3.25 mg/kg) (Covetrus North America, Cat: FP-001) was administered s.c. for
341 pain management. A single drop of topical Polytrim antibiotic (polymyxin B/trimethoprim;
342 Bausch & Lomb, Inc.) was administered after the irrigation. Mice were kept on the heating pad
343 until fully awake.
344
345 **Flow Cytometry**. Flow cytometry was used to test for FCRLS, to investigate Ly6C and CD45
346 expression, and to sort cells for ScRNAseq and ATAC-seq. Infiltrated monocytes were gated
347 as $CD45^{+}CD11b^{+}GFP^{+}$ cells and microglia is $CD45^{+}CD11b^{+}Cx3cr1^{+}GFP^{-}$. Using the
348 $CX3CR1^{+/GFP}$::$CCR2^{+/RFP}$ bone marrow transfer model, 1 day, 7 days and 1.5 months after
349 corneal alkali burn injury, mouse retinas were collected and single cell suspensions prepared
350 by papain digestion (Worthington Biochemical Corporation, Cat: LK003150). After digestion,
351 cells were blocked with CD16/32 (clone: 2.4G2) and stained with primary antibodies. Antibody
352 information can be found in **Table 1.** Samples were analyzed on a BD FACSAria^{TM} III cell
353 sorter and analyzed by FlowJo software.
354
355 **Single cell RNAseq and gene expression profiling:**
356 To perform drop-based encapsulation, flow sorted $CD45^{+}CD11^{+}$ cells were encapsulated into
357 micro droplets (≈50μm in diameter) using microfluidics (Fig. 6). The drops contain lysis buffer
358 and RNase inhibitor to maximize efficiency. Barcoded hydrogel beads, with template-
359 switching mastermix, were picoinjected into the droplets using high throughput microfluidic
360 pico-injector. Once the cDNA was synthesized in-drop by captured mRNA, the drops
361 (samples) were pooled and processed using Illumina HiSeq (deep sequencing) (Fig. 7). Cell
362 identification was performed using the unique sequencing index as well as DNA barcode,
363 during bioinformatic analysis. Library preparations of DNA for next generation sequencing
364 were made according to Klein et al [25]. Paired-end sequencing (100bp) was performed with
365 approximately 1,000 cells per sample on 1 lane of an Illumina HiSeq 2500. Reads were
366 preprocessed and analyzed as described in the preliminary studies except that a custom
367 reference transcriptome composed of the hg38 human reference transcriptome plus all BKV
368 transcripts was used during Bowtie mapping. Gene counts werre normalized to the total
369 number of mapped gene reads in each sample (RPM or reads per million). To confirm our

370 results, we also tested other normalization methods such as DESeq2 [26]. Ingenuity pathway
371 analysis (IPA®) from Qiagen was employed to understand the biological context of the single-
372 cell RNAseq data and identify major pathways, regulatory networks, and causal relationships
373 associated with the results.
374
375 **RNA isolation and Quantitative real-time PCR analysis**
376 A bone marrow transfer model was used to distinguish periphery infiltrated monocyte and
377 resident microglia. Naïve microglia cells and blood monocyte were collected from uninjured
378 bone marrow transferred mice. Injured microglia and engrafted monocyte were collected from
379 retinas 45 days after ocular injury in bone marrow transferred mice. Cells were directly
380 collected into 1ml Trizol (Thermo Fisher, Cat: 15596026). RNA extraction was performed per
381 standard assay recommendations Specifically, GlycoBlueTM Coprecipitant (Thermo
382 Fisher,Cat: AM9515) was added in the RNA precipitation step to help visualize the RNA pellet.
383 SMART-Seq V4 Ultra Low Input RNA Kit (Takara, Cat: 634890) was employed for RNA
384 reverse transcription and cDNA amplification. RNA from around 400 cells was loaded in the
385 experiment and 30ng cDNA could be yield after 18 cycles of cDNA amplification. cDNA
386 amount was measured with Qubit dsDNA Quantification Assay kit (High sensitivity) (Thermo
387 Fisher, Cat: Q32851). Quantitative real-time PCR analysis was conducted using TaqMan
388 Probes and TaqMan universal PCR Master Mix (Thermo Fisher, Cat: 4304437). 250pg-500
389 pg cDNA was loaded for each PCR reaction.
390
391
392 **ATAC-seq**
393 The $CX3CR1^{+/EGFP}$::$CCR2^{+/RFP}$ bone marrow transfer model was used to distinguish periphery
394 infiltrated monocyte and resident microglia. For flow sorting, infiltrated monocytes were gated
395 as $CD45^{+}CD11b^{+}GFP^{+}$ cells and microglia as $CD45^{+}CD11b^{+}CX3CR1^{+}GFP^{-}$. Each sample
396 was pooled from 5 retinas (from 5 mice) and 1000 to 5000 cells collected and used for ATAC-
397 seq analysis with the ATAC-seq kit from Active motif (Cat: 13150). Briefly, nuclei were isolated
398 by adding 100 µL ice cold ATAC-lysis buffer and then incubated with the tagmentation master
399 mix in a shaking heat block at 37°C/800 rpm for 30 min. Obtained DNA was purified and library
400 generated by PCR reaction for 13 cycles using indexed primers according to the

401 manufacturer's instructions. A quality control (QC) was performed to verify the size distribution
402 of the PCR enriched library fragments. ATAC-seq sequencing was performed on an Illumina
403 HiSeq 2000 instrument, resulting in 30 million paired-end 50 bp reads per sample. Reads
404 were mapped to the mm9 reference mouse genome using BWA [48]. Those fragments with
405 both ends unambiguously mapped to the genome that were longer than 100 bp were used for
406 further analysis. Hotspot2 was used to detect significant peaks with FDR cutoff of 0.05 [49].
407 For the analysis of overlap between peak regions, we used a cutoff of 50% reciprocal overlap
408 between the two compared regions. For the analysis of differential chromatin accessibility
409 between groups of replicate samples, DiffBind R package was used [50]:
410 (https://bioconductor.riken.jp/packages/3.2/bioc/vignettes/DiffBind/inst/doc/DiffBind.pdf).
411 Motif analysis was performed through MEME-CHIP (motif analysis of large nucleotide
412 datasets).
413
414 **Flat-Mount Staining and Imaging.**
415 1 day, 7 days and 1.5 months after corneal alkali burn injury, mouse retinas were collected
416 and prepared for staining and flat mount. Eyes were first fixed in 4% paraformaldehyde for 2
417 hours at room temperature. After dissection, retinas were blocked with blocking buffer for 1
418 hour at room temperature (PBS containing 5% normal donkey serum, 0.25% Triton-X-100).
419 Antibody information can be found in Table 1. For retinal flat-mount preparations, whole
420 retinas were laid flat after radial relaxing incisions and mounted on slides and cover-slipped.
421
422 **Acknowledgments**
423 This work was supported by the Boston Keratoprosthesis Research Fund, Department of
424 Defense (W81XWH2210774, W81XWH2010916), National Institute of Health
425 (7R01EY013124, 5P30EY003790), and the Retina Research Foundation (RRF).
426

427 **Figure Legends**

428 **Figure 1. Single-cell RNAseq analysis for retinal CD45$^+$CD11b$^+$ cells 0, 1, 4 and 7 days**
429 **after ocular injury. (A)** Principal component analysis shows the existence of 4 clusters with
430 distinct transcriptional profiles assigned to the day of cell retrieval. CD45$^+$CD11b$^+$ cells
431 undergo extensive changes in their transcriptome during retinal engraftment and by day 7
432 acquire an identical signature to naive microglia. **(B)** Singlec1$^+$ gene is expressed in clusters
433 3 and 4, both assigned to day 1, suggestive of the presence of monocytes within the microglia
434 sample. **(C)** tSNE analysis of CX3CR1, CCR2, P2ry12m Tmem119, Aif1, and Fcrls expression
435 in cluster 4 and **(D)** graphical representation of the expression of microglia markers P2ry12,
436 Tmem119, Aif1, and Fcrls in the 4 clusters, including those representatives of microglia and
437 monocytes signatures. **(E)** Flow cytometric analysis of the expression of CD45 marker in
438 retinal CX3CR1$^+$ cells before and 1, 4, and 7 days after injury. As reference we used a
439 CX3CR1$^{+/EFGP}$ mouse, stained with CD45 markers. Double positive CD45$^+$ CX3CR1$^+$ cells
440 represent only microglia, since naïve eyes do not have infiltration of monocytes[2]. To map
441 infiltrating/engrafting monocytes, we used a CX3CR1$^{+/EGFP}$ bone marrow chimera. CX3CR1$^+$
442 CD45$^+$ infiltrating monocytes gradually transitioned their CD45 expression towards the
443 expression of naïve microglia at 7 days.

444

445 **Figure 2. Protein expression of P2ry12, TMEM119 and FCRLS by engrafted**
446 **monocytes.**

447 CX3CR1$^{+/GFP}$::CCR2$^{+/RFP}$ bone marrow chimeras were used to differentiate engrafted
448 monocytes from embryonic microglia, followed by immunostaining and flow cytometry to
449 assess expression of P2ry12, TMEM119, and FCRLS proteins. **(A)** P2ry12 is not expressed
450 at day 1 and day 7 after monocyte infiltration into the retina, however 55% of GFP$^+$ engrafted
451 monocytes showed positive expression of P2ry12 at day 45. ***, $P < 0.001$.* **(B)** Twenty-five
452 percent of GFP$^+$ peripheral monocytes (white arrow) expressed TMEM119 at day 1. By day
453 7, all GFP$^+$ engrafted monocytes are TMEM119$^+$. TMEM119 expression in engrafted
454 monocytes is retained at day 45.**, $P < 0.01$; ***, $P < 0.001$.* **(C-D)** A CX3CR1$^{+/GFP}$::CCR2$^{+/RFP}$
455 bone marrow chimera was employed to assess Fcrls expression in monocytes and microglia
456 by flow cytometry. BMT CX3CR1$^+$ cells were labeled with a conjugated antibody against
457 CX3CR1 (BV605 or APC) which allowed differentiation between embryonic microglia

458 (BV605^{+}GFP^{-} or APC^{+}GFP^{-}) and engrafted monocytes (BV605^{+}GFP^{+} or APC^{+}GFP^{+}). Blood
459 monocytes had no Fcrls expression (grey). One day after infiltration, BV605^{+}GFP^{+} peripheral
460 monocytes (purple) acquired strong Fcrls expression, which was comparable to naïve
461 embryonic microglia. Fcrls expression was retained by engrafted monocytes sustained at day
462 7. At day 45, Fcrls expression was similar to embryonic microglia in the same injured tissue
463 or to naïve microglia. *, $P < 0.05$. *MFI: Median Fluorescence Intensity.* Yellow arrows indicate
464 GFP^{-} microglia and white arrows GFP^{+} engrafted monocytes. (A,B) *Scare bar = 50 μm.*
465

466 **Figure 3. ATAC-seq analysis to assess chromatin accessibility for P2ry12, FCRLS, Aif1**
467 **(IBA1), and TMEM119 genes in engrafted monocytes and microglia. (A)** Color coding of
468 analyzed groups. **(B)** P2ry12 gene contains 3 open chromatin peaks, 2 of the peaks (blue
469 arrowhead) are similar between the groups, but the 3rd peak is present in microglia (red
470 arrowhead) but not in circulating monocytes. Upon engraftment into the retina, monocytes
471 acquire the 3rd peak (red arrowhead) which is retained throughout the study period (45 days).
472 **(C)** Open chromatin peaks for Fcrls gene appear similar between the groups, with differences
473 only in the amplitude of the peaks at 45 days in microglia and engrafted monocytes which
474 have higher peaks compared to circulating monocytes or monocytes during early engraftment
475 into the retina (7 days). **(D)** Open chromatin peaks for Aif1 gene (IBA1) appear similar between
476 the groups, although microglia appeared to abolish one peak (red arrowhead) at 7 and 45
477 days after the injury. **(E)** TMEM119 has only one open chromatin peak, which is present in
478 microglia but not in circulating monocytes, but upon engraftment, peripheral monocytes
479 acquire this distinct peak (red arrowhead). **(F)** Heat map analysis of consensus peaks,
480 suggests that monocytes undergo significant open chromatin alterations upon engraftment
481 into the retina which allow differentiation from circulating monocytes. Monocytes increase
482 chromatin accessible for genes P2ry12, Tmem119, Fcrls, and Aif1 upon engraftment into the
483 retina eventually acquiring a similar open chromatin signature to microglia.
484

485 **Figure 4. ATAC-seq motif analysis for discovery of putative transcription factors**
486 **regulating monocyte engraftment.**
487 Motif analysis of differential open chromatin peaks identified by comparing naive microglia,
488 retinal engrafted monocyte (7 and 45 days), and circulating monocytes. Blue section contains

489 motifs assigned to transcription factors previously identified in human and mouse microglia,
490 such as PU.1 (most common), CTCF, IRF, RUNX, MEF2, C/EBP, AP-1, MAF, and MEF.
491 Green section contains enriched motifs assigned to novel transcription factors, such as
492 STAT1, FOXN1, KLFs, ATF3, and Npas4. Red section contains previously reported disease
493 associated motifs, such as MITF and NFKB1. Analysis of naive microglia identifies multiple
494 reported factors but not MAF and MEF, which are identified only in engrafted monocytes.
495 Engrafted monocyte at 7 and 45 days contain highly enriched motifs assigned to the above-
496 mentioned transcription factors CEBP, IRF2, and ATF3. Disease-associated motifs assigned
497 to MITF and NFKB1 are identified in engrafted monocytes but not in microglia. *E-value <0.05*
498 *for statistically significant motifs*.
499
500 **Figure 5. Expression of conventional markers by microglia and engrafted monocytes.**
501 **(A)** Development of a CX3CR1$^{+/GFP}$::CCR2$^{+/RFP}$ bone marrow chimera model to differentiate
502 microglia from peripheral monocytes using flow cytometry and a gating strategy as follows:
503 <u>microglia</u>: GFP$^{-negative}$ CX3CR1/BV605$^{+positive}$ or GFP$^{-negative}$ CX3CR1/APC$^{+positive}$, <u>engrafted</u>
504 <u>monocytes</u>: GFP$^{+positive}$CX3CR1/BV605$^{+positive}$ or GFP$^{+positive}$CX3CR1/APC$^{+positive}$. (B)
505 Peripheral monocyte/macrophages repress CCR2 expression and enhance CX3CR1
506 expression during engraftment into the retina. Five distinct maturation phases of monocytes
507 after engraftment are identified (Groups 1-5). A separate group of CCR$^{-negative}$CX3CR1$^{-negative}$
508 cells representing naive microglia (Group 6; μG) is retained as a population throughout the
509 study period (45 days). **(C-D)** Engrafted monocytes have increase expression of Ly6C at day
510 1 of infiltration, which is gradually suppressed during engraftment. At 45 days, the majority of
511 engrafted monocytes (Group 5) have similar Ly6G expression as microglia (Group 6). **(E-F)**
512 Engrafted monocytes exhibit sustained expression of CD45 at days 1 and 7 followed by
513 repression in subpopulations of these cells (Group 5), and at day 45 reaching equal levels
514 compared to retinal microglia (Group 6).
515
516 **Figure 6. Summary of the microglia and monocyte markers changes**
517 Monocyte transition from highly amoeboid to highly ramified cells during engraftment into the
518 retina, becoming morphometrically identical and indistinguishable from retinal microglia.
519 These changes are accompanied by suppression of monocyte markers CCR2, Ly6C, and

CD45, and upregulation of the tissue-resident macrophage marker CX3CR1$^{+/GFP}$ and microglia markers IBA1, TMEM119, P2ry12, and FCRLS. P2ry12 appears to be conditionally specific to microglia during early infiltration of monocytes) and to a subpopulation of engrafted monocytes.

Sup. Figure S1. mRNA expression of P2ry12, TMEM119, FCRLS, and IBA1 by blood monocytes, embryonic retinal microglia, and engrafted monocytes.

The CX3CR1$^{+/GFP}$ bone marrow transfer model was used to distinguish peripheral infiltrating monocytes from resident microglia. Naïve microglia cells and blood monocytes were collected from uninjured bone marrow transferred mice. Injured microglia and engrafted monocytes were collected from retinas 45 days after ocular injury in bone marrow transferred mice. Cells were collected using flow cytometry sorting with a gating strategy as follows: microglia: CD45^{+} CD11b^{+}GFP$^{-negative}$CX3CR1/BV605$^{+positive}$ or CD45^{+} CD11b^{+} GFP$^{-negative}$CX3CR1/APC$^{+positive}$, blood monocyte and engrafted monocytes: CD45^{+} CD11b^{+} GFP$^{+positive}$CX3CR1/BV605$^{+positive}$ or GFP$^{+positive}$CX3CR1/APC$^{+positive}$. RNA was isolated and mRNA expression of P2ry12, TMEM119, FCRLS and IBA1 genes was evaluated by PCR. P2ry12, TMEM119, and IBA1 mRNA level were normalized to blood monocyte, while the FCRLS mRNA level was normalized to naïve microglia. No FCRLS was detected in blood monocytes. This data indicates P2ry12, TMEM119, FCRLS, and IBA1 mRNA in engrafted monocytes is increased after retinal engraftment compared to blood monocytes.

Sup. Figure S2. Circulating monocytes do not express microglia makers.

Immunostaining of circulating blood monocytes from CX3CR1$^{+/GFP}$::CCR2$^{+/RFP}$ transgenic mice shows absence of P2ry12, IBA1, and TMEM119 expression. MHC II staining is present in engrafted monocytes. *Scare bar = 20 µm*

Sup. Figure S3. P2ry12 expression in engrafted monocyte at 14 days.

The CX3CR1$^{+/GFP}$::CCR2$^{+/RFP}$ bone marrow chimera model was employed to differentiate engrafted monocytes (GFP^{+}CCR2^{+}) from embryonic microglia (GFP^{-} CCR2^{-}). Peripheral monocytes acquired P2ry12 expression 14 days after engraftment into the retina. *Scale bar = 50 µm*.

551
552 **Sup. Figure S4.** Protein expression of Iba1 in engrafted monocytes.
553 The CX3CR1$^{+/GFP}$::CCR2$^{+/RFP}$ bone marrow chimera model was employed to differentiate
554 engrafted monocytes from embryonic microglia. Eighty-five percent of engrafted GFP^{+}
555 monocytes become IBA1^{+} at day 1 of infiltration, while all become IBA1^{+} at 7 and 45 days post
556 engraftment. *ns: Not significant. Yellow arrows indicate GFP$^{-negative}$ IBA1$^{+positive}$ microglia cells*
557 *and white arrows GFP$^{+positive}$ engrafted monocytes. Scare bar = 50 µm.*
558
559
560 **Table 1. Antibody information for flow Cytometry and immunostaining.**

ANTIBODY	FLUOROPHORE/SECONDARY	BRAND	CLONE	CATLOG NUMBER	DILUTION	APPLICATION
CD45	Brilliant Violet 785	Biolegend	30-F11	103149	1 to 100	Flow cytometry
CD11B	PerCP-Cyanine 5.5	Biolegend	M1/70	101228	1 to 100	Flow cytometry
LY6C	Brilliant Violet 421	Biolegend	HK1.4	128031	1 to 100	Flow cytometry
CX3CR1	APC	Biolegend	SA011F11	149008	1 to 100	Flow cytometry
CX3CR1	Brilliant Violet 605	Biolegend	SA011F11	149027	1 to 100	Flow cytometry
FCRLS	Alexa Fluor 647 donkey anti rat	Dr. Margeta			1 to 200	Flow cytometry
IBA1	Alexa Fluor 647 donkey anti rabbit	Wako		019-19741	1 to 300	Immunostaining
TMEM119	Alexa Fluor 647 donkey anti guinea pig	Synaptic systems		400 004	1 to 300	Immunostaining
P2RY12	Alexa Fluor 647 donkey anti rabbit	Dr. Margeta			1 to 200	Immunostaining
P2RY12	Alexa Fluor 647 donkey anti rabbit	Anaspec		as-55043a	1 to 200	Immunostaining
MHC-II	Alexa Fluor 647 donkey anti rat	BD Bioscience	I-A/I-E	556999	1 to 100	Immunostaining

561
562
563

Bibliography

1. Kamimura, D., et al., *The gateway theory: bridging neural and immune interactions in the CNS.* Front Neurosci, 2013. **7**: p. 204.
2. Paschalis, E.I., et al., *Permanent neuroglial remodeling of the retina following infiltration of CSF1R inhibition-resistant peripheral monocytes.* Proc Natl Acad Sci U S A, 2018. **115**(48): p. E11359-e11368.
3. Paschalis, E.I., et al., *The Role of Microglia and Peripheral Monocytes in Retinal Damage after Corneal Chemical Injury.* Am J Pathol, 2018. **188**(7): p. 1580-1596.
4. Paschalis, E.I., et al., *Microglia Regulate Neuroglia Remodeling in Various Ocular and Retinal Injuries.* J Immunol, 2019. **202**(2): p. 539-549.
5. Spiteri, A.G., et al., *Microglia and monocytes in inflammatory CNS disease: integrating phenotype and function.* Acta Neuropathol, 2022. **143**(2): p. 179-224.
6. Butovsky, O., et al., *Identification of a unique TGF-β-dependent molecular and functional signature in microglia.* Nat Neurosci, 2014. **17**(1): p. 131-43.
7. Bennett, M.L., et al., *New tools for studying microglia in the mouse and human CNS.* Proc Natl Acad Sci U S A, 2016. **113**(12): p. E1738-46.
8. Ronning, K.E., S.J. Karlen, and M.E. Burns, *Structural and functional distinctions of co-resident microglia and monocyte-derived macrophages after retinal degeneration.* J Neuroinflammation, 2022. **19**(1): p. 299.
9. Paschalis, E.I., et al., *Mechanisms of Retinal Damage after Ocular Alkali Burns.* Am J Pathol, 2017. **187**(6): p. 1327-1342.
10. Chen, X., et al., *Glaucoma after Ocular Surgery or Trauma: The Role of Infiltrating Monocytes and Their Response to Cytokine Inhibitors.* Am J Pathol, 2020. **190**(10): p. 2056-2066.
11. Galatro, T.F., et al., *Transcriptomic analysis of purified human cortical microglia reveals age-associated changes.* Nature Neuroscience, 2017. **20**(8): p. 1162-1171.
12. Gibbings, S.L., et al., *Three Unique Interstitial Macrophages in the Murine Lung at Steady State.* American Journal of Respiratory Cell and Molecular Biology, 2017. **57**(1): p. 66-76.
13. Fengyang, L., et al., *Single-cell RNA-seq reveals a dynamic shift of engrafted peripheral macrophages in the CNS towards a microglia signature.* 2021. **62**(8): p. 918-918.
14. Lei, F., et al., *CSF1R inhibition by a small-molecule inhibitor is not microglia specific; affecting hematopoiesis and the function of macrophages.* Proc Natl Acad Sci U S A, 2020. **117**(38): p. 23336-23338.
15. Saeed, S., et al., *Epigenetic programming of monocyte-to-macrophage differentiation and trained innate immunity.* Science, 2014. **345**(6204): p. 1251086.
16. Gibbings, S.L., et al., *Transcriptome analysis highlights the conserved difference between embryonic and postnatal-derived alveolar macrophages.* Blood, 2015. **126**(11): p. 1357-66.
17. van de Laar, L., et al., *Yolk Sac Macrophages, Fetal Liver, and Adult Monocytes Can Colonize an Empty Niche and Develop into Functional Tissue-Resident Macrophages.* Immunity, 2016. **44**(4): p. 755-68.
18. Gosselin, D., et al., *An environment-dependent transcriptional network specifies human microglia identity.* Science, 2017. **356**(6344).
19. Dolan, M.J., et al., *Exposure of iPSC-derived human microglia to brain substrates enables the generation and manipulation of diverse transcriptional states in vitro.* Nat Immunol, 2023. **24**(8): p. 1382-1390.
20. Rowan, S., et al., *Involvement of a gut-retina axis in protection against dietary glycemia-induced age-related macular degeneration.* Proc Natl Acad Sci U S A, 2017. **114**(22): p. E4472-E4481.

21. Wolf, S.A., H.W. Boddeke, and H. Kettenmann, *Microglia in Physiology and Disease.* Annu Rev Physiol, 2017. **79**: p. 619-643.
22. Benmamar-Badel, A., T. Owens, and A. Wlodarczyk, *Protective Microglial Subset in Development, Aging, and Disease: Lessons From Transcriptomic Studies.* Front Immunol, 2020. **11**: p. 430.
23. Zeng, J., et al., *The mechanism of microglia-mediated immune inflammation in ischemic stroke and the role of natural botanical components in regulating microglia: A review.* Front Immunol, 2022. **13**: p. 1047550.
24. Choi, I., et al., *Autophagy enables microglia to engage amyloid plaques and prevents microglial senescence.* Nat Cell Biol, 2023. **25**(7): p. 963-974.
25. Lv, Q.K., et al., *Role of alpha-synuclein in microglia: autophagy and phagocytosis balance neuroinflammation in Parkinson's disease.* Inflamm Res, 2023. **72**(3): p. 443-462.
26. Zhou, C., et al., *Sustained Inhibition of VEGF and TNF-α Achieves Multi-Ocular Protection and Prevents Formation of Blood Vessels after Severe Ocular Trauma.* Pharmaceutics, 2023. **15**(8).
27. Satoh, J., et al., *TMEM119 marks a subset of microglia in the human brain.* Neuropathology, 2016. **36**(1): p. 39-49.
28. Walker, D.G., et al., *Patterns of Expression of Purinergic Receptor P2RY12, a Putative Marker for Non-Activated Microglia, in Aged and Alzheimer's Disease Brains.* Int J Mol Sci, 2020. **21**(2).
29. Vankriekelsvenne, E., et al., *Transmembrane protein 119 is neither a specific nor a reliable marker for microglia.* Glia, 2022. **70**(6): p. 1170-1190.
30. Vanneste, D., et al., *MafB-restricted local monocyte proliferation precedes lung interstitial macrophage differentiation.* Nat Immunol, 2023. **24**(5): p. 827-840.
31. Kenkhuis, B., et al., *Co-expression patterns of microglia markers Iba1, TMEM119 and P2RY12 in Alzheimer's disease.* Neurobiol Dis, 2022. **167**: p. 105684.
32. Sideris-Lampretsas, G., et al., *Galectin-3 activates spinal microglia to induce inflammatory nociception in wild type but not in mice modelling Alzheimer's disease.* Nat Commun, 2023. **14**(1): p. 3579.
33. Matek, W., et al., *Initial experience with the new electronic endoscope.* Endoscopy, 1984. **16**(1): p. 20-1.
34. Haimon, Z., et al., *Cognate microglia-T cell interactions shape the functional regulatory T cell pool in experimental autoimmune encephalomyelitis pathology.* Nat Immunol, 2022. **23**(12): p. 1749-1762.
35. Stratoulias, V., et al., *ARG1-expressing microglia show a distinct molecular signature and modulate postnatal development and function of the mouse brain.* Nat Neurosci, 2023. **26**(6): p. 1008-1020.
36. Wu, Q., et al., *Microglial activation and over pruning involved in developmental epilepsy.* J Neuropathol Exp Neurol, 2023. **82**(2): p. 150-159.
37. Yin, Z., et al., *Identification of a protective microglial state mediated by miR-155 and interferon-gamma signaling in a mouse model of Alzheimer's disease.* Nat Neurosci, 2023. **26**(7): p. 1196-1207.
38. Chen, X., et al., *Microglia-mediated T cell infiltration drives neurodegeneration in tauopathy.* Nature, 2023. **615**(7953): p. 668-677.
39. O'Koren, E.G., R. Mathew, and D.R. Saban, *Fate mapping reveals that microglia and recruited monocyte-derived macrophages are definitively distinguishable by phenotype in the retina.* Sci Rep, 2016. **6**: p. 20636.
40. Hammond, T.R., et al., *Single-Cell RNA Sequencing of Microglia throughout the Mouse Lifespan and in the Injured Brain Reveals Complex Cell-State Changes.* Immunity, 2019. **50**(1): p. 253-271 e6.
41. Zhou, N., et al., *Transcriptional mechanism of IRF8 and PU.1 governs microglial activation in neurodegenerative condition.* Protein Cell, 2019. **10**(2): p. 87-103.

655 42. Fixsen, B.R., et al., *SALL1 enforces microglia-specific DNA binding and function of SMADs to*
656 *establish microglia identity.* Nat Immunol, 2023. **24**(7): p. 1188-1199.
657 43. Kierdorf, K., et al., *Bone marrow cell recruitment to the brain in the absence of irradiation or*
658 *parabiosis bias.* PLoS One, 2013. **8**(3): p. e58544.
659 44. Skene, P.J., J.G. Henikoff, and S. Henikoff, *Targeted in situ genome-wide profiling with high*
660 *efficiency for low cell numbers.* Nat Protoc, 2018. **13**(5): p. 1006-1019.
661 45. Dresselhaus, E.C. and M.K. Meffert, *Cellular Specificity of NF-κB Function in the Nervous System.*
662 Front Immunol, 2019. **10**: p. 1043.
663 46. Saban, D.R., *New concepts in macrophage ontogeny in the adult neural retina.* Cell Immunol, 2018.
664 **330**: p. 79-85.
665 47. Yu, C., et al., *Microglia versus Monocytes: Distinct Roles in Degenerative Diseases of the Retina.*
666 Trends Neurosci, 2020. **43**(6): p. 433-449.
667 48. Li, H. and R. Durbin, *Fast and accurate short read alignment with Burrows-Wheeler transform.*
668 Bioinformatics, 2009. **25**(14): p. 1754-60.
669 49. John, S., et al., *Chromatin accessibility pre-determines glucocorticoid receptor binding patterns.* Nat
670 Genet, 2011. **43**(3): p. 264-8.
671 50. Ross-Innes, C.S., et al., *Differential oestrogen receptor binding is associated with clinical outcome in*
672 *breast cancer.* Nature, 2012. **481**(7381): p. 389-93.
673

Figure 1

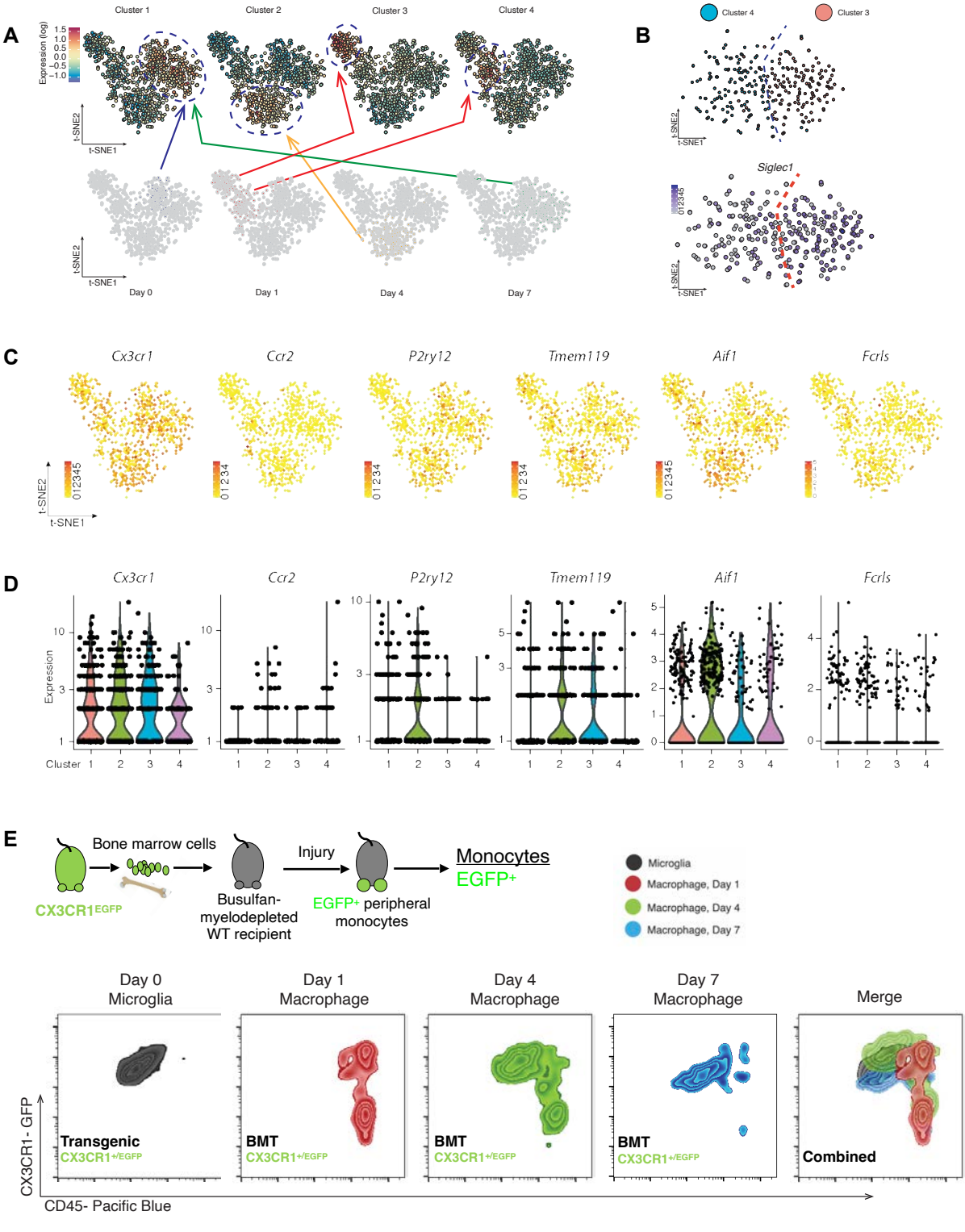
A
Cluster 1
Cluster 2
Cluster 3
Cluster 4
Expression (log)
t-SNE2
t-SNE1
Day 0
Day 1
Day 4
Day 7
B
Cluster 4
Cluster 3
Siglec1
C
Cx3cr1
Ccr2
P2ry12
Tmem119
Aif1
Fcrls
D
Expression
Cluster
E
Bone marrow cells
CX3CR1EGFP
Busulfan-myelodepleted WT recipient
Injury
EGFP+ peripheral monocytes
Monocytes
EGFP+
Microglia
Macrophage, Day 1
Macrophage, Day 4
Macrophage, Day 7
Day 0 Microglia
Day 1 Macrophage
Day 4 Macrophage
Day 7 Macrophage
Merge
Transgenic
CX3CR1+/EGFP
BMT
CX3CR1+/EGFP
BMT
CX3CR1+/EGFP
BMT
CX3CR1+/EGFP
Combined
CX3CR1- GFP
CD45- Pacific Blue

Figure 2

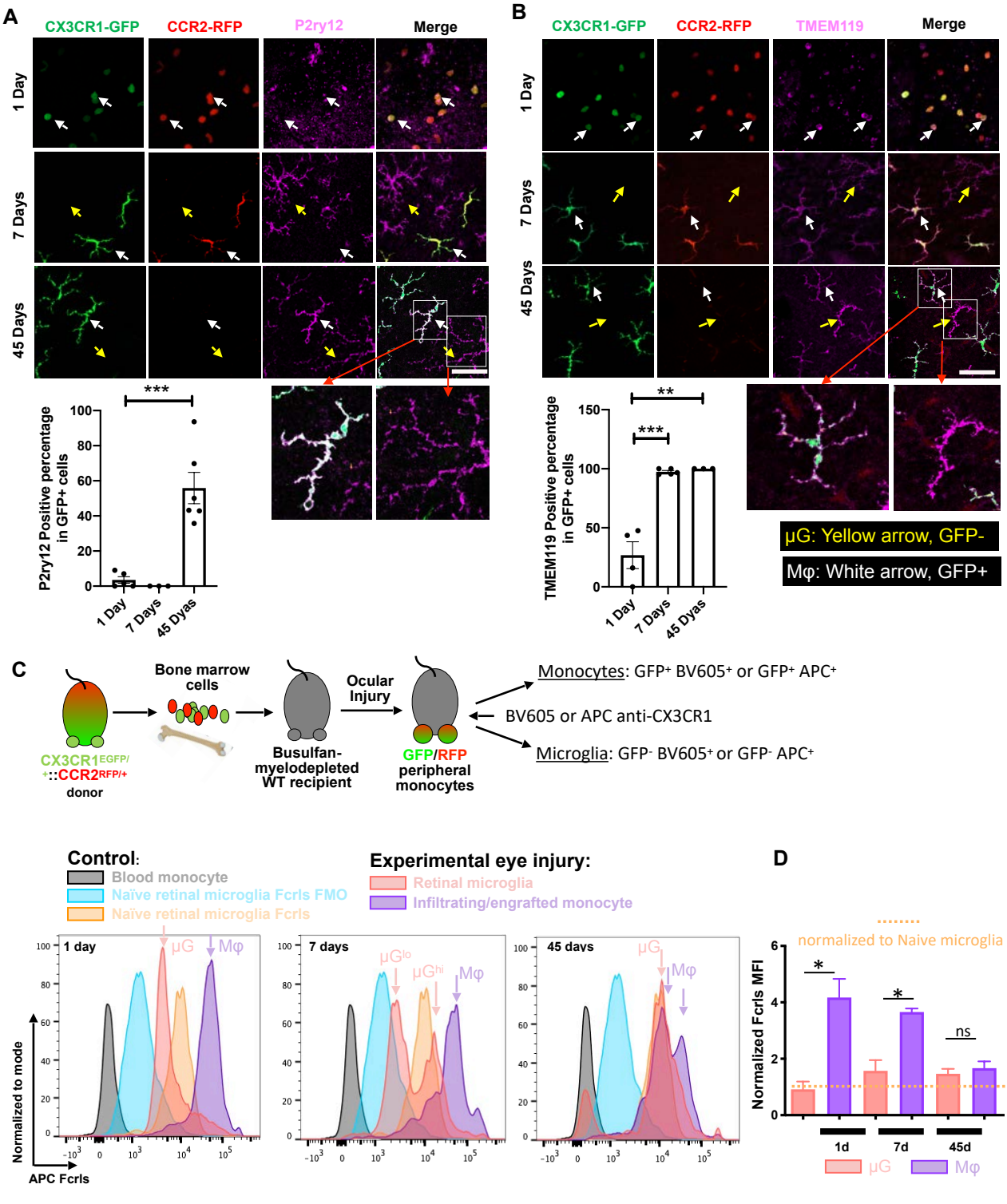
A
CX3CR1-GFP
CCR2-RFP
P2ry12
Merge
1 Day
7 Days
45 Days
P2ry12 Positive percentage in GFP+ cells
***
1 Day
7 Days
45 Dyas
B
CX3CR1-GFP
CCR2-RFP
TMEM119
Merge
TMEM119 Positive percentage in GFP+ cells
**
***
μG: Yellow arrow, GFP-
Mφ: White arrow, GFP+
C
Bone marrow cells
Ocular Injury
CX3CR1EGFP/+::CCR2RFP/+ donor
Busulfan-myelodepleted WT recipient
GFP/RFP peripheral monocytes
Monocytes: GFP+ BV605+ or GFP+ APC+
BV605 or APC anti-CX3CR1
Microglia: GFP- BV605+ or GFP- APC+
Control:
Blood monocyte
Naïve retinal microglia FcrIs FMO
Naïve retinal microglia FcrIs
Experimental eye injury:
Retinal microglia
Infiltrating/engrafted monocyte
1 day
7 days
45 days
μG
Mφ
μGlo
μGhi
Normalized to mode
APC FcrIs
D
normalized to Naive microglia
Normalized FcrIs MFI
ns
1d
7d
45d
μG
Mφ

Figure 3

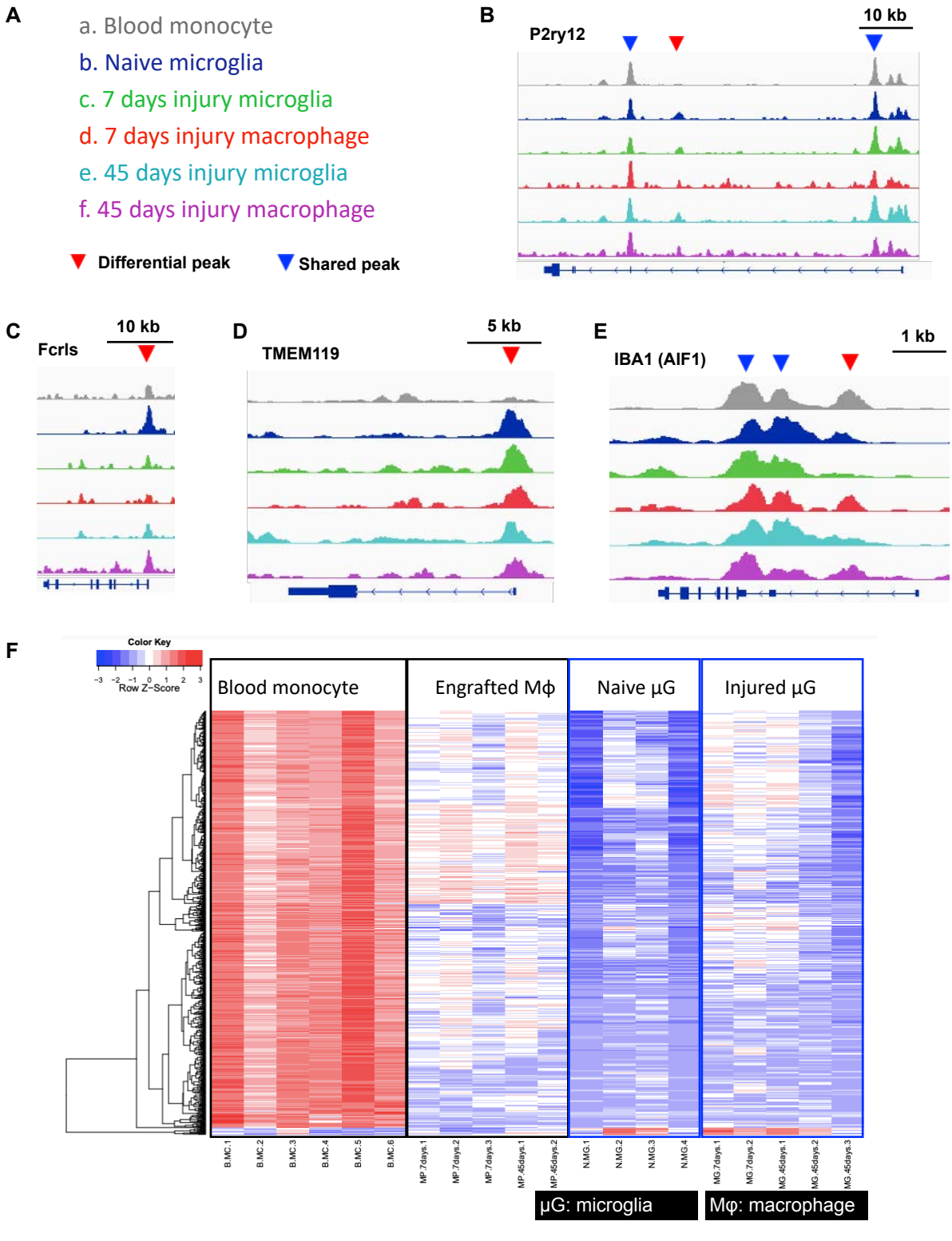
A
a. Blood monocyte
b. Naive microglia
c. 7 days injury microglia
d. 7 days injury macrophage
e. 45 days injury microglia
f. 45 days injury macrophage
Differential peak
Shared peak
B
P2ry12
10 kb
C
Fcrls
10 kb
D
TMEM119
5 kb
E
IBA1 (AIF1)
1 kb
F
Color Key
Row Z-Score
Blood monocyte
Engrafted Mϕ
Naive μG
Injured μG
B.MC.1
B.MC.2
B.MC.3
B.MC.4
B.MC.5
B.MC.6
MP.7days.1
MP.7days.2
MP.7days.3
MP.45days.1
MP.45days.2
N.MG.1
N.MG.2
N.MG.3
N.MG.4
MG.7days.1
MG.7days.2
MG.45days.1
MG.45days.2
MG.45days.3
μG: microglia
Mϕ: macrophage

Figure 4

(comparing μG/ 7days Mφ/45 days Mφ to blood monocyte)

Motif	Best Match	Naive μG	7 day Mφ	45 day Mφ	
	PU.1	+	+	+	Corroborate previous identified microglia motif
	CTCF	+	-	+	
	RUNX	+	+	-	
	AP-1	+	+	+	
	CEBP	+	-	-	
	IRF2	+	-	-	
	MAF	-	+	+	
	MEF	-	+	-	
	STAT1	+	+	+	Newly identified motif
	FOXN1	+	-	+	
	KLF5/9	+	+	-	
	Atf3	+	-	-	
	Npas4	+	+	-	
	MITF	-	+	+	Disease associated motif
	NFKB1	-	+	-	

Significant Motifs (E-values ≤ 0.05)

μG: microglia

Mφ: macrophage

Figure 5

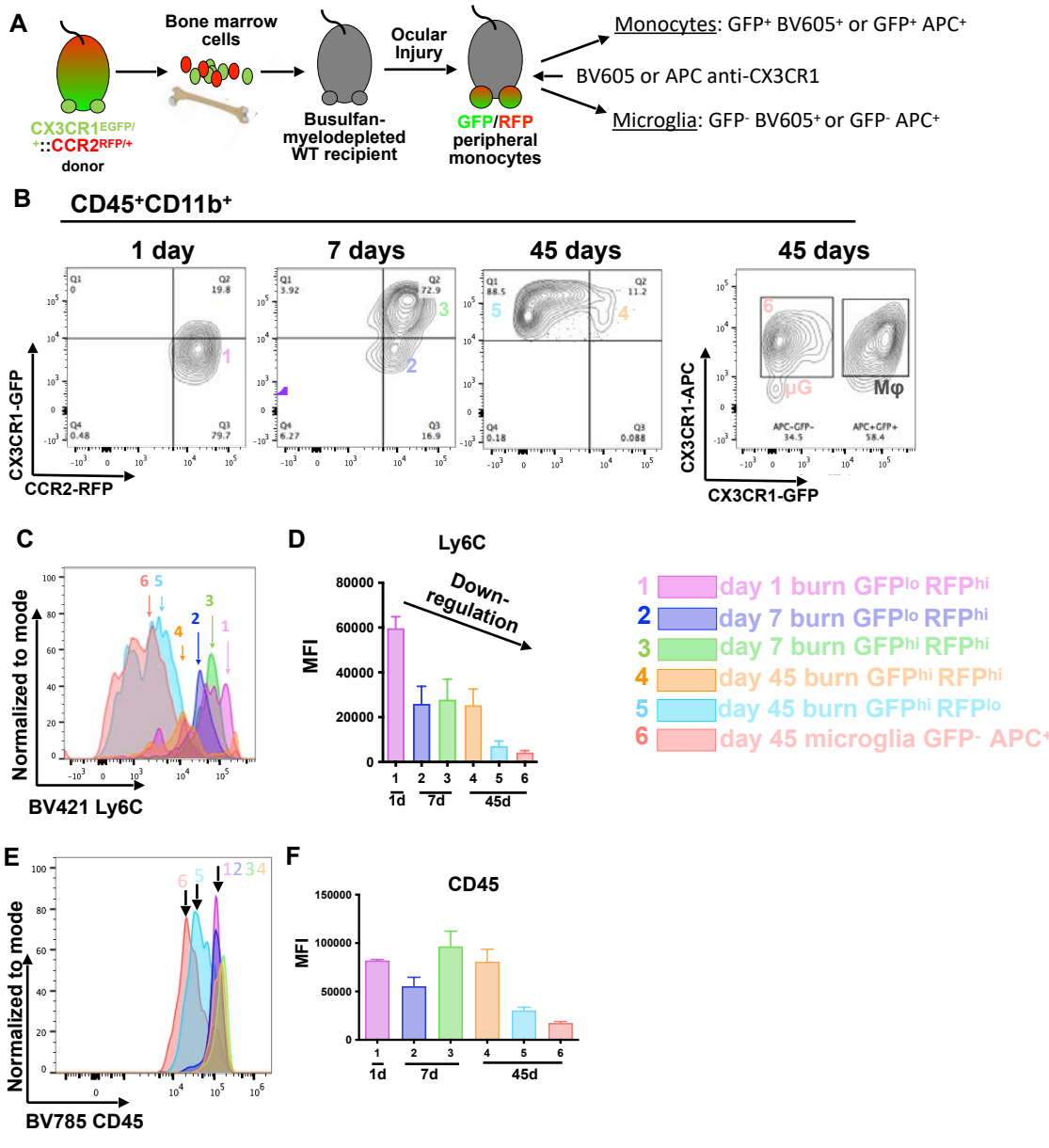
A
Bone marrow cells
Ocular Injury
CX3CR1EGFP/+::CCR2RFP/+ donor
Busulfan-myelodepleted WT recipient
GFP/RFP peripheral monocytes
Monocytes: GFP+ BV605+ or GFP+ APC+
BV605 or APC anti-CX3CR1
Microglia: GFP- BV605+ or GFP- APC+
B
CD45+CD11b+
1 day
7 days
45 days
45 days
CX3CR1-GFP
CCR2-RFP
CX3CR1-APC
CX3CR1-GFP
μG
Mφ
C
Normalized to mode
BV421 Ly6C
D
Ly6C
MFI
Down-regulation
1d
7d
45d
1 day 1 burn GFPlo RFPhi
2 day 7 burn GFPlo RFPhi
3 day 7 burn GFPhi RFPhi
4 day 45 burn GFPhi RFPhi
5 day 45 burn GFPhi RFPlo
6 day 45 microglia GFP- APC+
E
Normalized to mode
BV785 CD45
F
CD45
MFI
1d
7d
45d

Figure 6

	YS µG	Engrafted Mφ		
		1 day	7 days	45 days
	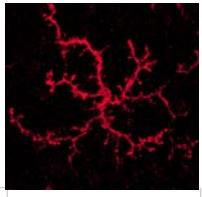	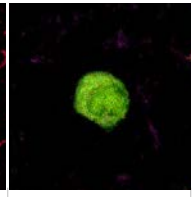	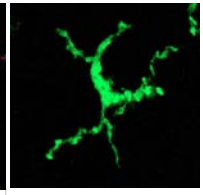	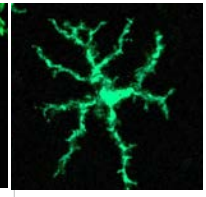
Cell-type	**YS µG** Ramified/ small soma	**Mφ** Ameboid/ large soma	**Mφ** Semi-ramified/ large soma	**Mφ** Ramified/ large soma
IBA1	**+**	**+**	**+**	**+**
TMEM119	**+**	**Lo**	**+**	**+**
P2ry12	**+**	**-**	**-**	**Lo/Hi***
Fcrls	**+**	**Hi**	**Hi**	**+/Hi**
CCR2	-	Hi	Low	-
CX3CR1	+	Lo	Lo/Hi*	Hi
Ly6C	-	Hi	Hi	-/Lo*
CD45	Int	Hi	Hi	Int/Hi *

**** Heterogeneous***

Sup. Figure S1

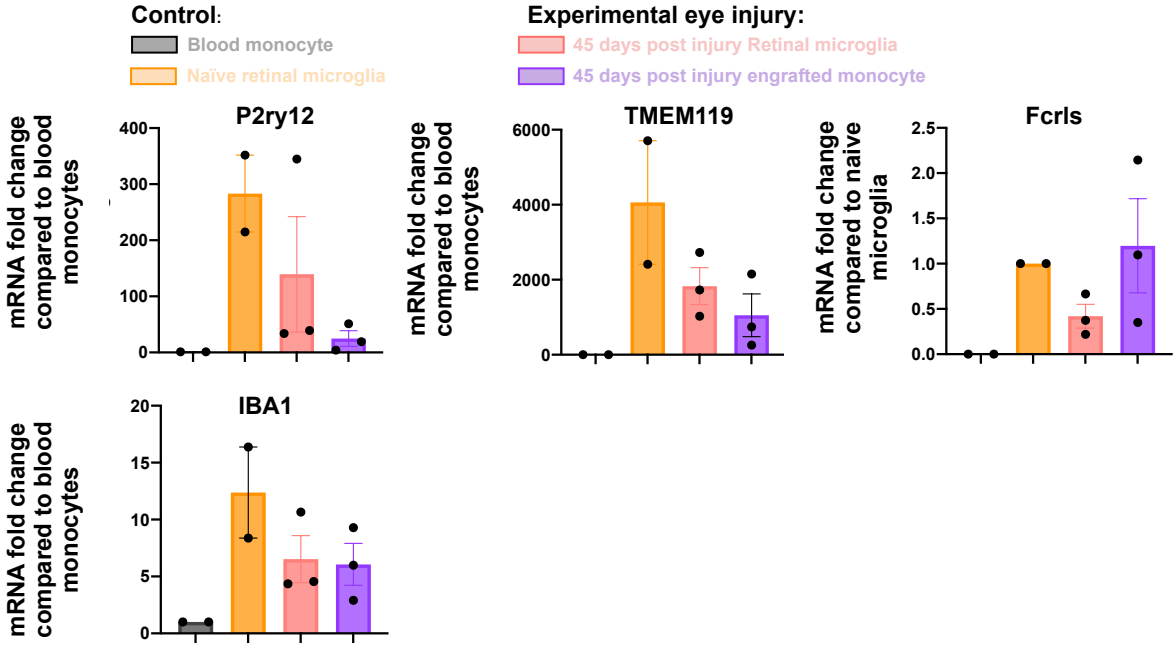

Sup. Figure S2

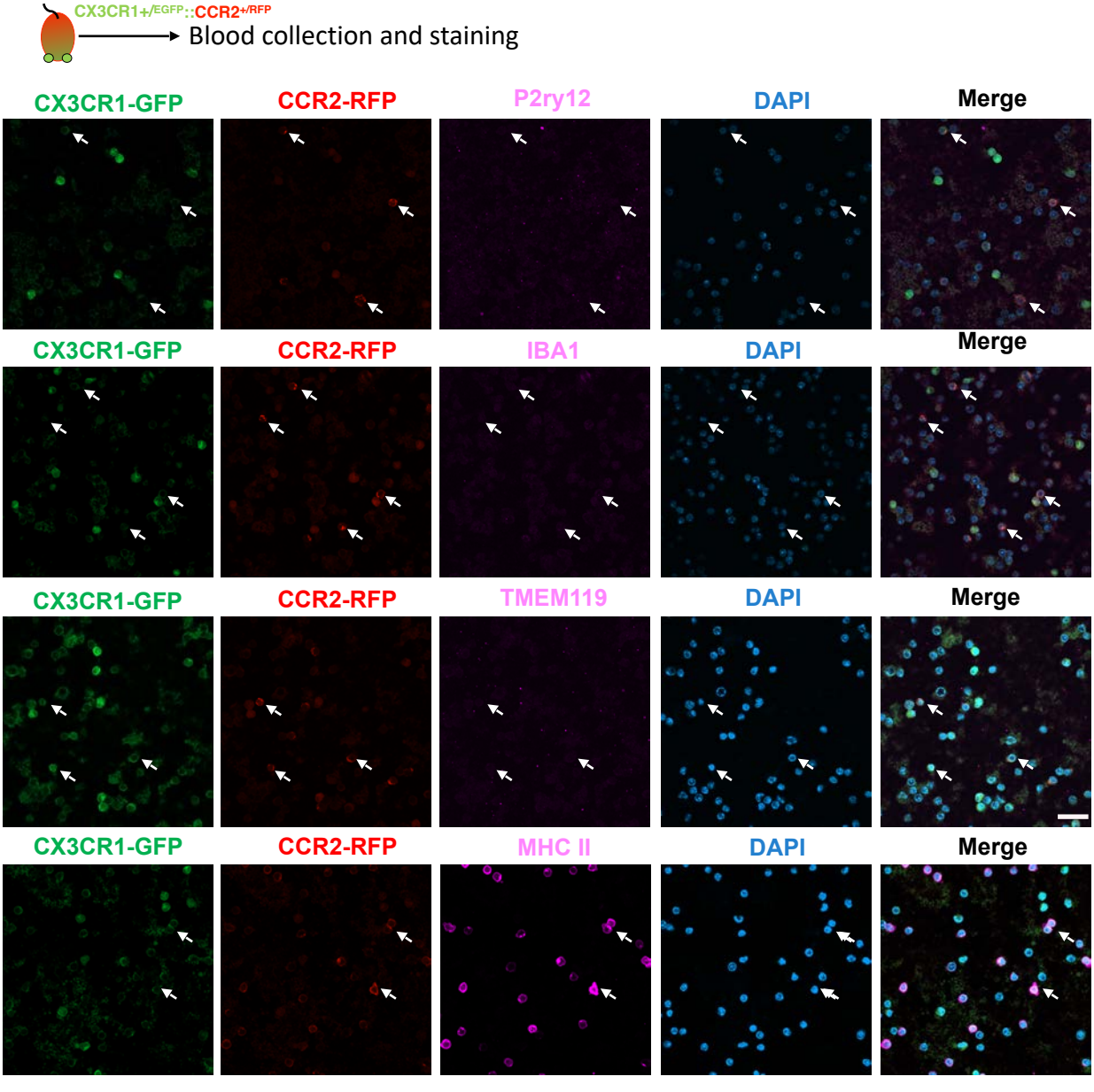

Sup. Figure S3

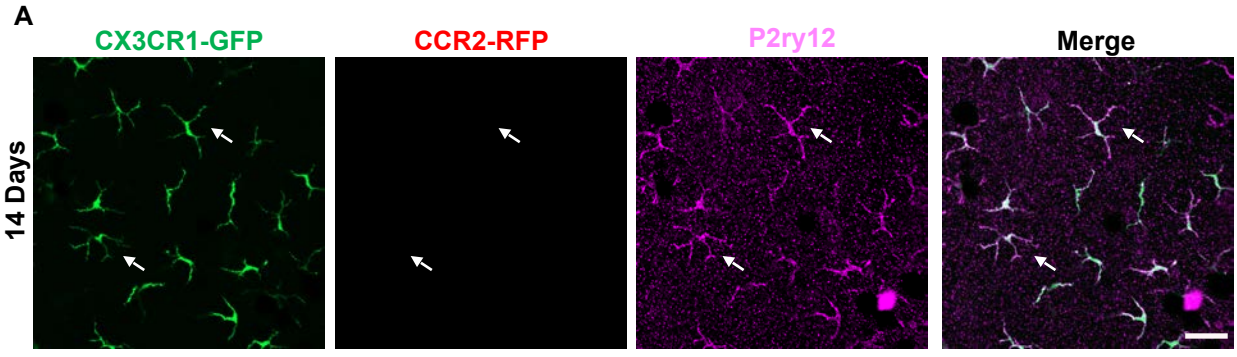
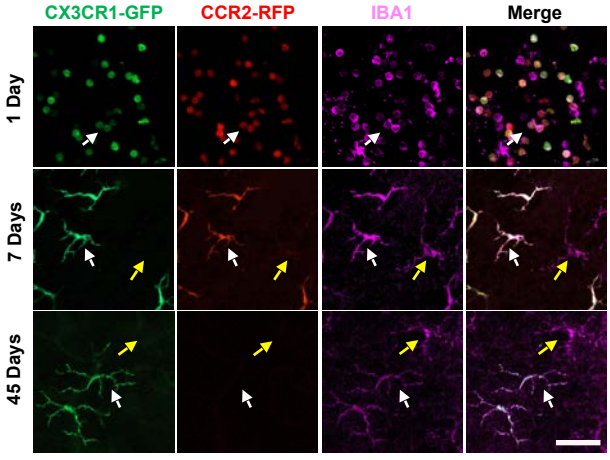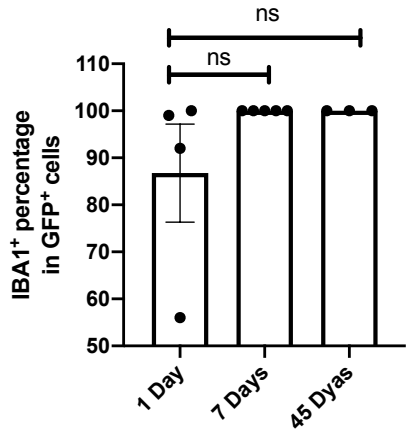
Sup. Figure S4